The Asymmetry Parameter of Cirrus Clouds Composed of Hollow Bullet Rosette–Shaped Ice Crystals from Ray-Tracing Calculations

C. G. SCHMITT

National Center for Atmospheric Research, Boulder, Colorado*

J. IAQUINTA+

Division for Metrology and Instrumentation, French Public Works Research Laboratory, Paris, France

A. J. HEYMSFIELD

National Center for Atmospheric Research, Boulder, Colorado*

(Manuscript received 9 May 2005, in final form 24 October 2005)

ABSTRACT

Cirrus clouds in the midlatitude and Arctic regions are often composed of bullet rosette–shaped ice crystals. Bullet rosette–shaped ice crystals are composed of a number of bullets radiating from a central point. The bullets that make up the rosette will grow to be hollow in some conditions. To understand better the radiative impact of cirrus clouds, the authors have used a ray-tracing code to calculate the scattering properties of solid and hollow bullet rosettes at visible wavelengths. Results show that hollow bullet rosettes exhibit a broader forward-scattering peak than do solid bullet rosettes. This difference results in an asymmetry parameter that is as much as 0.08 lower for hollow bullet rosettes than for solid rosettes. The effective asymmetry parameter of spheres with the same particle volume and total surface area of the bullet rosettes has also been calculated. Asymmetry parameter estimates for equivalent spheres were similar to those calculated using the ray tracing. Asymmetry parameter calculations were used in combination with direct aircraft measurements from the Atmospheric Radiation Measurement Program intensive operational period in March of 2000. Asymmetry parameter estimates were used with particle size distributions for three cirrus cloud flights for which the observed large particles were predominantly bullet rosettes. Calculated asymmetry parameter values (0.80–0.84) agreed poorly with published cirrus parameterizations (0.75–0.84) when applied to the same aircraft data. Differences lead to 4.5–9 W m^{-2} differences in reflected and transmitted visible light energy for a cloud of 0.5 optical depth.

1. Introduction

Cirrus clouds regularly cover about 30% of the globe (Wylie et al. 1994) and are an important component of the earth's radiation budget (Liou and Takano 1994). They have been identified as one of the most uncertain components regulating the earth's climate (Liou 1986; Stephens et al. 1990; Lynch et al. 2002). The radiative behavior of such clouds depends on the microphysical properties of the cloud particles (Kristjansson et al. 2000). Observations from aircraft two-dimensional cloud probes and balloonborne replicators show that the majority of particles in midlatitude and polar cirrus clouds are composed of bullet rosette–shaped ice crystals (Heymsfield and Knollenberg 1972; Heymsfield and Platt 1984; Sassen et al. 1995). Bailey and Hallett (2004) showed that bullet rosettes are likely to be hollow when supersaturations are high, a common condition in particle-growing regions of cirrus clouds (Heymsfield and Miloshevich 1995). Bailey and Hallett (2004) also showed that bullet rosettes will become increasingly hollow when they fall into warmer regions that are more conducive to plate growth.

* The National Center for Atmospheric Research is sponsored by the National Science Foundation.

+ Current affiliation: Transport Research Laboratory, Wokingham, Berkshire, United Kingdom.

Corresponding author address: Carl Schmitt, P.O. Box 3000, Boulder, CO 80307.
E-mail: schmittc@ucar.edu

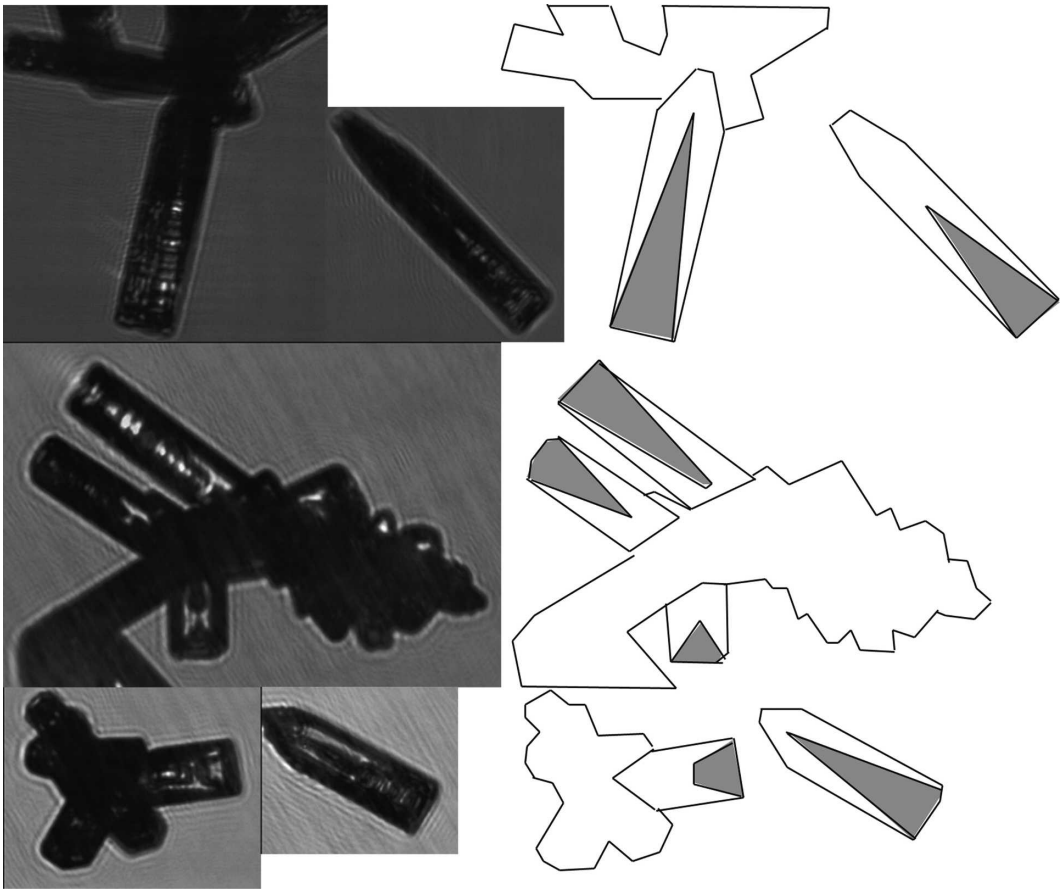

FIG. 1. Several examples of bullet rosettes observed with the CPI, along with corresponding outlines highlighting the hollow bullets.

The occurrence of hollowness in cirrus-cloud bullet rosettes was shown in Heymsfield (1972). Individual bullets were photographed and then melted, and the resulting drops were measured to determine their weight. Hollow bullets can be identified as bullets that have densities less than the density of ice. Analysis of these data showed that 84% of the bullets studied had some degree of hollowness, while 30% had low enough densities that their hollowness factor was 1.0, meaning that the longest possible six-sided pyramid of ice was missing from the bullet.

Hollow bullet rosette images are frequently seen in the literature. Some can be seen in replicator data shown in Heymsfield et al. (2002) and Heymsfield (1972). With the advent and frequent use of the Stratton Park Engineering Company, Inc. (SPEC, Inc.), Cloud Particle Imager (CPI) probe, it is more commonly possible to observe the hollowness of bullet rosettes. Figure 1 shows some hollow ice particles imaged in midlatitude cirrus with the CPI during the Atmospheric Radiation Measurement Program intensive operational period (ARM IOP) in 2000.

The radiative multiple-scattering properties of atmospheric ice crystals are often investigated using ray tracing of theoretical ice particle shapes (Fu 1996, hereinafter Fu96; Takano and Liou 1989; Yang and Liou 1997). These studies have focused mainly on simple ice crystal shapes such as columns and plates, although Takano and Liou (1995) and Macke et al. (1996) studied more complex shapes such as capped columns, hollow columns, and simple dendrites and Yang and Liou (1998) studied dendrites, sector plates, and fractals. Particles with significant concavities have rarely been studied because of the added complexity of allowing rays to exit and reenter the particle. Mitchell et al. (1996) studied irregular polycrystals, which had concavities but were more compact than bullet rosettes. Iaquinta et al. (1995), Takano and Liou (1995), and Yang and Liou (1998) have studied solid bullet rosettes.

A commonly derived factor used to represent the scattering properties of particles is the asymmetry parameter. The asymmetry parameter is defined as the average cosine of the scattering angle, weighted by the intensity of the total scattered light and is commonly

used in two-stream radiative multiple-scattering models (Mitchell et al. 1996). Results from Takano and Liou (1995) show that the asymmetry parameter for differently shaped ice particles at visible wavelengths can vary from 0.80 to 0.90 while solid and hollow columns, which are commonly found in cirrus, were 0.8429 and 0.8576, illustrating that particle hollowness can lead to considerable differences in asymmetry parameter. This difference in asymmetry parameter will lead to a difference in radiative forcing of 2 W m^{-2} (calculation to be discussed in aircraft application section) for visible wavelengths at cloud top, assuming an optical-depth-0.5 cloud with a sun angle 35° from vertical. For comparison, radiative forcing on the order of 4 W m^{-2} is expected by the doubling of atmospheric carbon dioxide in greenhouse gas studies (Cess et al. 1993).

Spheres of an effective size (referred to as "equivalent spheres") are often used in substitution for ice particle populations when calculating ice-cloud scattering properties (Neshyba et al. 2003). This is a convenient strategy because of the simplicity of Mie theory in comparison with ray-tracing calculations. Equivalent spheres with the same total volume and total surface area as the ice particle being simulated (hereinafter referred to as EVSA spheres) were used by Grenfell and Warren (1999). Results of extinction, asymmetry parameter, and single-scattering albedo calculations using EVSA spheres agree well with ray-tracing calculations for simple plates and columns (Neshyba et al. 2003).

Climate models require accurate parameterizations of the scattering properties of cirrus clouds (Fu96). Ray-tracing results have been used to develop parameterizations of these properties (Fu96; Fu and Liou 1993). These studies used simple hexagonal particles for their calculations. The use of bullet rosette–shaped ice crystal properties would be more realistic for midlatitude and Arctic cirrus.

In this study, the authors investigate the asymmetry parameter of hollow bullet rosette ice crystals and apply the results to aircraft data for comparison with other parameterizations. In section 2, a ray-tracing program is used to calculate the scattering properties of hollow rosettes. In section 3, the results from the ray-tracing study are compared with equivalent sphere asymmetry parameter estimates. In section 4, the results of the ray-tracing study are applied to aircraft measurements and compared with other asymmetry parameter parameterizations. Conclusions are discussed in section 5.

2. Ray-tracing study

The ray-tracing code used in this project is described completely in Iaquinta et al. (1995). The ray-tracing code calculates the scattering phase function of the ice crystal using a Monte Carlo geometric ray-tracing approach. The ray-tracing method sends separate rays of light to hit the modeled ice crystal. The light rays travel along straight lines independently from one another (Liou and Hansen 1971). Interference between rays within the particle was neglected given the added complexity of this calculation. When a ray interacts with a particle surface, the direction and intensity of the reflected and refracted rays are calculated using Snell's law. In this study, crystal surfaces are assumed to be smooth and absorption is considered to be negligible to simulate visible light scattering. Internally reflected rays are followed until less than 1% of the initial energy remains. A total of 1 000 000 rays were used: 50 rays were sent for each of the 20 000 orientations of the crystals.

Diffraction is computed using the actual two-dimensional shadow of each orientation of the bullet rosette. According to Babinet's principle, the distribution of light intensity diffracted by an object is identical to that refracted by an aperture corresponding to its two-dimensional projection perpendicular to the incident beam. The effect caused by light diffracted by one bullet intersecting with another bullet was ignored. For details on the calculation of the diffraction see Iaquinta et al. (1995).

This ray-tracing study concentrated on a single crystal type while the aspect ratio (width/length) and the hollowness of the bullets were varied. A rosette with six bullets uniformly spaced in three dimensions was chosen as being representative of atmospheric bullet rosettes (Heymsfield et al. 2002). The bullet rosette used in this study has the same bullet orientation as the 6–3 configuration in Iaquinta et al. (1995). The Iaquinta et al. (1995) study showed that the number of bullets and bullet-to-bullet geometry did not significantly affect asymmetry parameter values. Iaquinta et al. (1995) showed that the asymmetry parameter for bullet rosettes with solid bullets varies by less than 1% (from 0.831 to 0.839) for 11 different particle orientations varying from single bullets to rosettes with eight bullets.

Figure 2 shows a few random orientations of the 6–3 bullet rosettes. To create the hollow portion of the bullet rosette, a six-sided prism was removed from the ends of each of the six bullets. The hollowness factor was calculated as the ratio of the prism length divided by the total length of the bullet. Figure 2 also shows several individual bullets with varying degrees of hollowness. The hollowness factor was varied from 0 to 1.0 and the aspect ratio of the bullets was also varied from 0.1 to 1.0. In this study, the exterior shape of the considered hollow bullets is identical to that of the solid

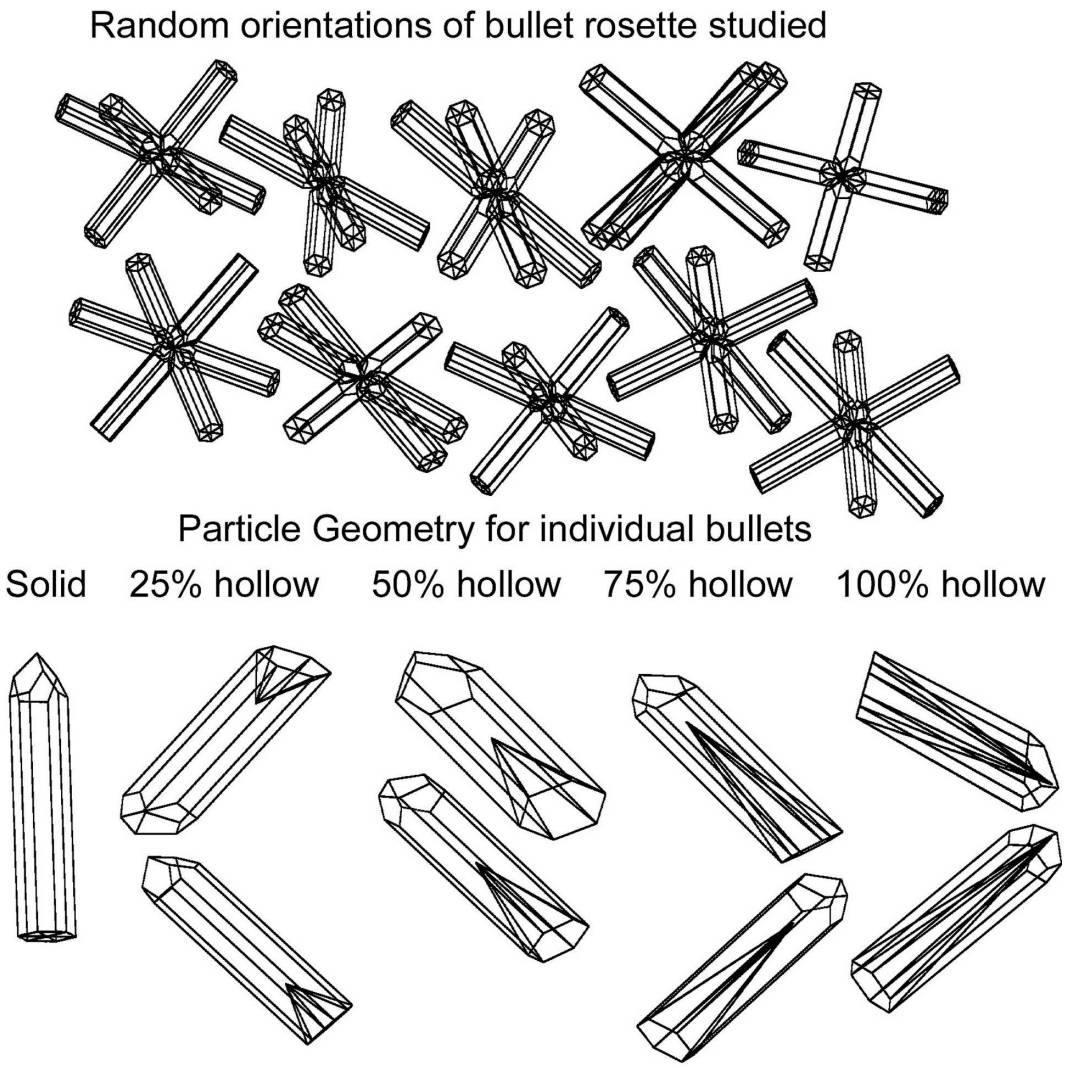

FIG. 2. The geometry of the studied bullet rosette is shown with several random orientations. Detailed images of theoretical individual bullets with varying degrees of hollowness are also shown.

bullets. The elementary solid bullet has 10 faces—3 pentagonal faces that make up the point, 6 sides, three of which are rectangles and three of which are elongated pentagons, and the hexagonal end.

The scattering phase function was calculated for bullet rosettes composed of bullets with different hollowness factors and aspect ratios. Figure 3 shows the scattering phase function for two bullet rosettes with bullet aspect ratios of 0.25. The top graph shows the phase function for the rosette with solid bullets, and the bottom graph shows the phase function for a rosette with hollow bullets (hollowness factor 1.0). Note that the forward diffraction peak is plotted, though it is very narrow and therefore difficult to see. The forward-scattering peak between 2° and 20° for the hollow bullet rosette is stronger than for the solid rosette. This difference is likely due to a small change to the direction of light rays that occurs when passing through the end of a hollow bullet.

The asymmetry parameter was directly derived from the scattering phase function by multiplying by the cosine of the phase angle. Integrating the phase function using a trapezoidal rule was found to be sufficient with 1° angular resolution. Figure 4 shows the asymmetry parameter for bullet rosettes with varying degrees of hollowness and aspect ratios. Results from long skinny bullets (aspect ratios of 0.1) are represented by the top curve. Aspect ratios increase with each successively lower curve. The hollowness factor progresses from solid on the left to hollow on the right. Calculations preformed on individual bullets confirmed the asymmetry parameter trends observed for the hollow bullet

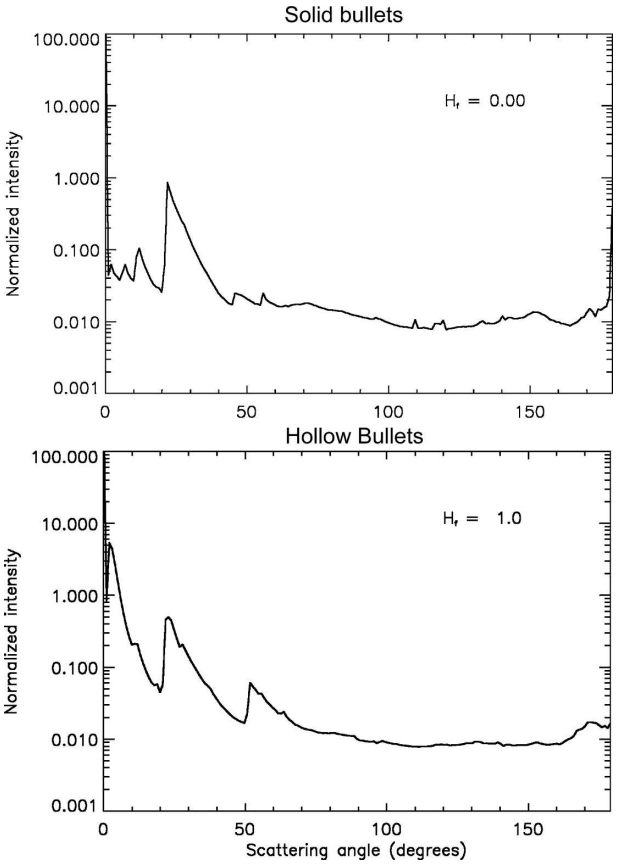

FIG. 3. Scattering phase function calculated for bullet rosettes with (top) solid and (bottom) hollow bullets.

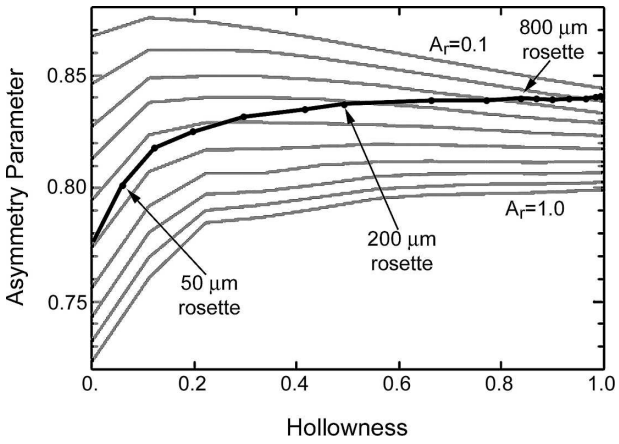

FIG. 4. The asymmetry parameter for the modeled bullet rosettes vs hollowness. The lowest curve represents the asymmetry parameter of rosettes with high-aspect-ratio bullets, and the uppermost curve shows the asymmetry parameter of rosettes with long skinny bullets. The thick curve shows asymmetry parameter values for bullet rosettes with typical aspect ratios and hollowness values. Hollowness was varied from 0 to 1.

rosettes, because the results were comparable. The largest difference in asymmetry parameter resulting from hollowness is for the high-aspect-ratio bullets, but all aspect ratios show significant variations. This demonstrates that hollow bullet rosettes have distinctly different scattering properties than do solid bullet rosettes.

Heymsfield (1972) measured the aspect ratio and density of bullets in bullet rosette ice crystals and derived a function to estimate aspect ratio by size for cirrus particles. These experimental results have been used to estimate where commonly occurring cirrus particles would fall on Fig. 4. A line representing the values for common cirrus-cloud bullet rosette properties is shown as the thick line on Fig. 4. The data show that typical bullet rosettes larger than 300 μm would have an asymmetry parameter that is nearly constant at a value of 0.84, whereas smaller bullet rosettes should have asymmetry parameters decreasing to as low as 0.78 for sub-50-μm particles.

The scattering properties of the hollow bullet rosettes are different because some of the energy included in the delta transmission peak (light that passes directly through parallel surfaces of a particle with no change in direction) of solid bullet rosettes will scatter in other than a forward direction if the bullets are hollow. Surfaces of the hollow region being nearly parallel to exterior surfaces results in a broadening of the forward scattering peak as shown in Fig. 3, because some energy from the delta transmission peak is scattered at low angles. Energy lost from the delta transmission peak will undergo a larger change in direction for less hollow particles because the angle difference with the interior surfaces of the hollow region will be larger.

3. Equivalent spheres

Equivalent sphere populations having equal total volume and equal total surface area were calculated for each of the modeled rosettes. This technique, first advanced by Grenfell and Warren (1999) and Neshyba et al. (2003), leads to a large number of spheres being used to represent single ice particles. Equivalent sphere sizes calculated to represent the studied bullet rosettes varied in size from 12-μm diameter for hollow bullet rosettes with low-aspect-ratio bullets to 116 μm for solid bullet rosettes with high-aspect-ratio bullets. For spheres of these sizes, the asymmetry parameter at visible wavelengths is 0.87–0.89 as calculated by Mie theory. These values clearly do not agree with the ray-tracing results shown in Fig. 4 (0.87–0.73). This is because bullet rosettes are being represented by a collection of EVSA spheres. The interior surfaces of the hol-

low regions are represented by exterior surfaces of the spheres (Neshyba et al. 2003). This causes the spheres to have a larger projected area than individual bullet rosettes. The resulting asymmetry parameter from the equivalent spheres must therefore be adjusted to account for the projected area differences between the bullet rosette and spheres. This is done by using a similarity relationship developed by Liou (2002) to relate alternative representations of scatterers in radiative multiple scattering. The relationship was derived for the purpose of achieving similar multiple-scattering results using different single-scattering properties such as the asymmetry parameter. The relationship is

$$\tau_1\omega_1(1 - g_1) = \tau_2\omega_2(1 - g_2), \quad (1)$$

where τ is the optical depth, ω is the single-scattering albedo, and g is the asymmetry parameter. The subscripts 1 and 2 represent the two particle populations being compared (in this situation, bullet rosettes and equivalent spheres). Because the ray-tracing technique applied here used visible-wavelength ice scattering properties, the authors are assuming that there is no absorption, meaning that the single-scattering albedo is 1.0. This leads to

$$\tau_r(1 - g_1) = (1 - g_2), \quad (2)$$

where τ_r is the ratio of the optical depth of the equivalent spheres to the optical depth of the bullet rosette. For the particles under consideration, the optical depth is equal to 2 times the projected area (the geometric optics approximation). Calculation of the projected area for the bullet rosettes was done by averaging the two-dimensional projected area from 10 000 random orientations of the bullet rosettes. The application of Eq. (2) to the dataset improved the equivalent sphere asymmetry parameter estimates significantly, though the result should not be taken as a substitution for multiple-scattering calculations, which are beyond the scope of this study. Figure 5 compares the value for the two different sides of Eq. (2). The 1:1 line is drawn to aid the eye. The stars represent particles with aspect ratios and hollowness values that are typically observed in midlatitude cirrus based on the parameterizations from Heymsfield (1972).

The EVSA theory asymmetry parameter estimates predicted values that were in the same range as the ray-tracing values, though the one-to-one correspondence was poor. Restricting the dataset to commonly observed bullet rosette geometries (represented by stars) did not improve the correlation. Taken directly, the EVSA calculations predict that the smaller bullet rosettes would have higher asymmetry parameter values, while the larger bullet rosettes would have lower values. These results are contrary to the ray-tracing results.

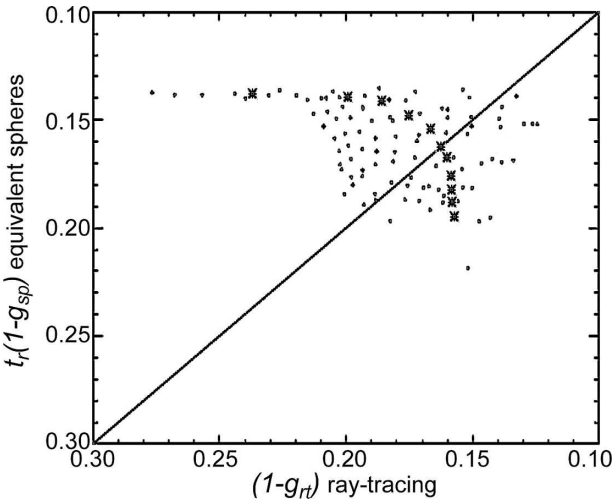

FIG. 5. The value $\tau_r(1 - g_{sp})$ for equivalent sphere methods plotted vs $(1 - g_{rt})$ of hollow rosettes from ray tracing, comparing the utility of the equivalent sphere theory to predict the asymmetry parameter. The stars represent values for typical hollowness and aspect-ratio values for cirrus.

4. Application to aircraft data

Cirrus-cloud asymmetry parameter values were estimated using aircraft particle size distribution and ice water content measurements from aircraft data. During the ARM IOP in March of 2000, the University of North Dakota (UND) Citation aircraft sampled cirrus clouds that were primarily composed of bullet rosette–shaped ice crystals on 3 days. Samples of the CPI particle imagery for the aircraft study can be seen in Heymsfield et al. (2002). For particle size distribution measurements, particles larger than 45 μm in maximum dimension were measured with the Particle Measuring Systems, Inc., (PMS) two-dimensional cloud probe (2D-C; 33–1000 μm) and the PMS two-dimensional precipitation probe (2D-P; 200–6000 μm). The techniques used to calculate the raw size distribution data from the 2D-C and 2D-P are discussed in Heymsfield et al. (2002). The PMS Forward-Scattering Spectrometer Probe (FSSP) was used for measurement of size distributions for particles smaller than 45 μm. The counterflow virtual impactor (CVI) probe was used for the measurement of ice water content. The CVI directly measures the condensate mass of all particles larger than approximately 7 μm in diameter. The probe measures condensed water contents from about 0.005 (Twohy et al. 1997) to about 1 g m^{-3}. The uncertainty in the condensed water content is about 11% at 0.2 g

m^{-3} and increases to 23% at 0.01 g m^{-3}. Asymmetry parameter estimates were not made when the CVI measurements were less than 0.01 g m^{-3}. Particle size distributions and ice water content measurements were averaged over a period of 1 min of in-cloud time, yielding 160 valid data points over the 3 days of flights.

Asymmetry parameter estimates have been calculated for size distributions by scaling the ray-tracing values by the projected area for each size bin. For particles smaller than 45 μm, the asymmetry parameter of droxtals (Zhang et al. 2004) was used. Zhang et al. (2004) calculated the asymmetry parameter for two droxtal geometries. Results using both values are included in this study. The asymmetry parameters for the most likely bullet aspect ratio and hollowness were used for larger particles (from the thick line in Fig. 4). The FSSP concentrations may be overestimated because of the breakup of large ice particles on the inlet of the probe (Field et al. 2003), as well as ice particle sizing uncertainties. The effect of this possible overcounting of small particles was investigated by reducing the number of FSSP particles by one-half. The resulting asymmetry parameter was less than 0.01 lower than when the full FSSP distribution was included.

The aircraft measurement asymmetry parameter value estimates were generally between 0.80 and 0.84 for the particle size distributions. These results are compared with the Fu96 parameterization for cirrus clouds at visible wavelengths. The Fu96 parameterization is based on the generalized effective diameter (D_{ge}) of size distributions. Equation (3) shows the formula for D_{ge}:

$$D_{ge} = \frac{2(3)^{1/2}}{3\rho_i}\frac{\mathrm{IWC}}{A_c}, \tag{3}$$

where D_{ge} is the generalized effective diameter, IWC is the measured ice water content, ρ_i is the density of ice, and A_c is the measured projected area.

For comparison with current calculations, D_{ge} was calculated using the IWC value from the CVI as well as the total particle projected area from the aircraft particle probes. The D_{ge} values ranged from 20 to 230 μm with a mean of 70 μm. For comparison, the Fu96 parameterization for the scattering properties of cirrus between 440 and 480 nm was used. The Fu96 parameterization and the hollow rosette asymmetry parameter estimates (using the two different asymmetry parameter values for droxtals) are compared in Fig. 6. The difference between the Fu96 parameterization and the bullet rosette estimates is likely because the Fu96 parameterization is based on ray tracing of solid hexagonal columns that had high aspect ratios (0.8) for particles smaller than 87.5 μm. High-aspect-ratio columns have a lower asymmetry parameter than do small rosettes [about 0.77 for 1.0-aspect-ratio columns from Macke et al. (1996) as compared with 0.78–0.82 for small rosettes in the same size range from this study]. This leads the Fu96 parameterization to predict lower asymmetry parameter values for particle size distributions dominated by small particles. One of the droxtal geometries has an asymmetry parameter comparable to that of the high-aspect-ratio columns, but because the droxtal asymmetry parameter values were only used for particle sizes up to 45 μm, the results were not improved.

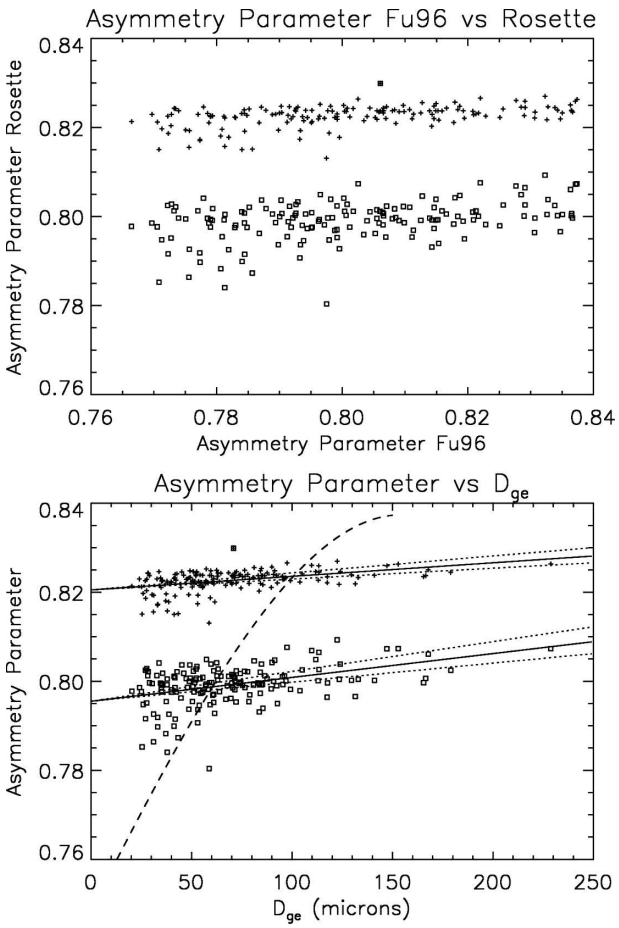

FIG. 6. Midlatitude cirrus asymmetry parameters. (top) The asymmetry parameter from the hollow bullet rosette calculations vs that of the Fu96 parameterization for March 2000 ARM cirrus flights. Plus signs indicate calculations using an asymmetry parameter for droxtals of 0.8038, and squares indicate calculations using a value of 0.7459. (bottom) The same asymmetry parameter values plotted vs the generalized mean diameter D_{ge}. The solid lines show linear fits to the aircraft calculations. The dotted lines show potential errors caused by aircraft measurement errors in the calculation of D_{ge}. The dashed line shows the asymmetry parameter calculated from the Fu96 parameterization for 440–480 nm.

Figure 6 also shows the bullet rosette asymmetry parameter values plotted against D_{ge}. The bullet rosette asymmetry parameter was calculated twice, using the two different droxtal asymmetry parameter values. Equations (4a) and (4b) are the equations for the trend lines shown in the figure for droxtal asymmetry parameter values of 0.8038 and 0.7459, respectively:

$$g = 0.821 + (3.05 \times 10^{-5})D_{ge} \quad \text{and} \tag{4a}$$

$$g = 0.796 + (5.35 \times 10^{-5})D_{ge}. \tag{4b}$$

Each of the bullet rosette trend lines has a dotted line above and below it representing the potential error based on a 25% combined error in the D_{ge} calculation caused by errors in the aircraft probe data. The dashed line shows the Fu96 parameterization for 440–480 nm. Fu96 did not study particle size distributions with D_{ge} values larger than 130 μm.

The effect of the different asymmetry parameter value estimates can be investigated using atmospheric radiative transfer equations. For thin clouds, Coakley and Chylek (1975) applied the two-stream approximation to the radiative transfer equation to obtain relationships for the reflectance and transmittance of energy through a plane-parallel atmosphere. The two-stream approximations were found to agree with numerical solutions of the radiative transfer equations for layers with optical depths of 0.5 and below. The equations for reflectance and transmittance for a nonabsorbing cloud are

$$R(\mu) = \frac{\tau(1-g)}{2\mu + \tau(1-g)} \quad \text{and} \tag{5}$$

$$T(\mu) = 1 - r(\mu), \tag{6}$$

where $R(\mu)$ is the reflectance, $T(\mu)$ is the transmittance, τ is the cloud optical depth, g is the asymmetry parameter, and μ is the cosine of the angle of incidence of the sun.

The sun emits 640 W m^{-2} of energy between 380 and 780 nm. A 0.5-optical-depth cloud composed of bullet rosettes and droxtals would have significantly different radiative properties than if the asymmetry parameter were based on the Fu96 parameterization. For a particle size distribution with a D_{ge} value of 25 μm, the bullet rosette parameterization produces a radiative forcing difference of 4.5–9 W m^{-2} depending on which droxtal asymmetry value is assumed for a sun incident angle of 35° from vertical. The differences drop with D_{ge} values between 50 and 100 μm and then increase again with larger D_{ge} values.

5. Summary

Bullet rosette–shaped ice crystals are frequently observed in cirrus-cloud microphysical data. Laboratory experiments as well as aircraft data show that these bullet rosettes can develop hollow bullets in common cirrus conditions. Determining the influence of hollow bullet rosettes on the cirrus-cloud radiative properties is important for increased understanding of the role of cirrus clouds in climate. The scattering properties of hollow bullet rosettes have been computed with a ray-tracing code and estimated using equivalent spheres. The results of the equivalent sphere asymmetry parameter estimates were scattered within the same range as the ray-tracing values; however, the results showed no common trends. The results from the ray-tracing code were applied to aircraft data collected during cirrus-cloud flights for which bullet rosettes were the most frequently observed particle type. The asymmetry parameter calculated from the aircraft data was compared with the Fu96 parameterization. The comparison shows that the Fu96 parameterization predicts lower asymmetry parameter values when smaller particles dominated the size distribution.

Acknowledgments. This research was supported by NASA Grant L16441. The authors thank the crew of the UND Citation.

REFERENCES

Bailey, M., and J. Hallett, 2004: Growth rates and habits of ice crystals between −20° and −70°C. *J. Atmos. Sci.,* **61,** 514–544.

Cess, R. D., and Coauthors, 1993: Uncertainties in carbon dioxide radiative forcing in atmospheric general circulation models. *Science,* **262,** 1252–1255.

Coakley, J. A., and P. Chylek, 1975: The two-stream approximation in radiative transfer: Including the angle of the incident radiation. *J. Atmos. Sci.,* **32,** 409–418.

Field, P. R., R. Wood, P. R. A. Brown, P. H. Kaye, E. Hirst, R. Greenaway, and J. A. Smith, 2003: Particle interarrival times measured with a Fast FSSP. *J. Atmos. Oceanic Technol.,* **20,** 249–261.

Fu, Q., 1996: An accurate parameterization of the solar radiative properties of cirrus clouds for climate models. *J. Climate,* **9,** 2058–2082.

——, and K. N. Liou, 1993: Parameterization of the radiative properties of cirrus clouds. *J. Atmos. Sci.,* **50,** 2008–2025.

Grenfell, T. C., and S. G. Warren, 1999: Representation of nonspherical ice particles by a collection of independent spheres for scattering and absorption of radiation. *J. Geophys. Res.,* **104,** 31 697–31 709.

Heymsfield, A. J., 1972: Ice crystal terminal velocities. *J. Atmos. Sci.,* **29,** 1348–1357.

——, and R. G. Knollenberg, 1972: Properties of cirrus generating cells. *J. Atmos. Sci.,* **29,** 1358–1366.

——, and C. M. R. Platt, 1984: A parameterization of the particle

size spectrum of ice clouds in terms of the ambient temperature and the ice water content. *J. Atmos. Sci.,* **41,** 846–855.

——, and L. M. Miloshevich, 1995: Relative humidity and temperature influences on cirrus formation and evolution: Observations from wave clouds and FIRE II. *J. Atmos. Sci.,* **52,** 4302–4326.

——, S. Lewis, A. Bansemer, J. Iaquinta, L. Milosovich, M. Kajikawa, C. Twohy, and M. Poellot, 2002: A general approach for deriving the properties of cirrus and stratiform ice cloud particles. *J. Atmos. Sci.,* **59,** 3–29.

Iaquinta, J., H. Isaka, and P. Personne, 1995: Scattering phase function of bullet rosette ice crystals. *J. Atmos. Sci.,* **52,** 1401–1413.

Kristjansson, J. E., J. M. Edwards, and D. L. Mitchell, 2000: The impact of a new scheme for the optical properties of ice crystals on the climate of two GCMs. *J. Geophys. Res.,* **105,** 10 063–10 079.

Liou, K. N., 1986: Influence of cirrus clouds on weather and climate processes: A global perspective. *Mon. Wea. Rev.,* **114,** 1167–1199.

——, 2002: *An Introduction to Atmospheric Radiation*. 2d ed. Academic Press, 583 pp.

——, and J. E. Hansen, 1971: Intensity and polarization for single scattering by polydisperse spheres: A comparison of ray optics and Mie theory. *J. Atmos. Sci.,* **28,** 995–1004.

——, and Y. Takano, 1994: Light scattering by nonspherical particles: Remote sensing and climate implications. *Atmos. Res.,* **31,** 271–298.

Lynch, D. K., K. Sassen, D. O'C. Starr, and G. Stephens, Eds., 2002: *Cirrus*. Oxford University Press, 480 pp.

Macke, A., J. Mueller, and E. Raschke, 1996: Single scattering properties of atmospheric ice crystals. *J. Atmos. Sci.,* **53,** 2813–2825.

Mitchell, D. L., A. Macke, and Y. Liu, 1996: Modeling cirrus clouds. Part II: Treatment of radiative properties. *J. Atmos. Sci.,* **53,** 2967–2988.

Neshyba, S. P., T. C. Grenfell, and S. G. Warren, 2003: Representation of a nonspherical ice particle by a collection of independent spheres for scattering and absorption of radiation: 2. Hexagonal columns and plates. *J. Geophys. Res.,* **108,** 4448, doi:10.1029/2002JD003302.

Sassen, K., and Coauthors, 1995: The 5–6 December 1991 FIRE IFO II jet stream cirrus case study: Possible influences of volcanic aerosols. *J. Atmos. Sci.,* **42,** 97–123.

Stephens, G. L., S. C. Tsay, P. W. Stackhouse, and P. J. Flatau, 1990: The relevance of the microphysical and radiative properties of cirrus clouds to climate and climate feedback. *J. Atmos. Sci.,* **47,** 1742–1753.

Takano, Y., and K. N. Liou, 1989: Solar radiative transfer in cirrus clouds. Part I: Single-scattering and optical properties of hexagonal ice crystals. *J. Atmos. Sci.,* **46,** 3–19.

——, and ——, 1995: Radiative transfer in cirrus clouds. Part III: Light scattering by irregular ice particles. *J. Atmos. Sci.,* **52,** 818–837.

Twohy, C. H., A. J. Schanot, and W. A. Cooper, 1997: Measurement of condensed water content in liquid and ice clouds using an airborne counterflow virtual impactor. *J. Atmos. Oceanic Technol.,* **14,** 197–202.

Wylie, D. P., W. P. Menzel, H. M. Woolf, and K. I. Strabala, 1994: Four years of global cirrus cloud statistics using HIRS. *J. Climate,* **7,** 1972–1986.

Yang, P., and K. N. Liou, 1997: Light scattering by hexagonal ice crystals: Solutions by a ray-by-ray integration algorithm. *J. Opt. Soc. Amer.,* **14,** 2278–2289.

——, and ——, 1998: Single-scattering properties of complex ice crystals in terrestrial atmosphere. *Contrib. Atmos. Phys.,* **71,** 223–248.

Zhang, Z., P. Yang, G. W. Kattawar, S. Tsay, B. A. Baum, Y. Hu, A. J. Heymsfield, and J. Reichardt, 2004: Geometrical-optics solution to light scattering by droxtal ice crystals. *Appl. Opt.,* **43,** 2490–2499.